Optica Applicata, Vol. XLVIII, No. 3, 2018
10.5277/oa180309

Study on self-repairing and non-diffraction of Airy beams in slant atmospheric turbulence

Ya-Qing Li*, Li-Guo Wang

School of Optoelectronic Engineering, Xi'an Technological University, Xi'an 710021, China

*Corresponding author: liyaqing0401@163.com

The Airy beams propagation in atmospheric turbulence along a slant path was simulated numerically, based on the split-step Fourier method. Also, the self-repairing and non-diffraction characteristics of Airy beams were investigated and compared with beams propagation on a horizontal path. The effects of parameters including zenith angle, propagation distance, radii of Gaussian aperture and turbulence intensity on the two characteristics of beams were revealed. Additionally, the two characteristics of the Airy beam were compared with those of a Bessel–Gauss beam. The results showed that the two beams obscured by Gaussian apertures can be repaired after propagating some distance along a slant path. However, the non-diffraction characteristic of an Airy beam was stronger than that of a Bessel–Gauss beam and the amplitude attenuation rate of the Bessel–Gauss beam was greater than that of the Airy beam in the process of self-repairing. Results obtained can provide a theoretical basis for an outdoor experiment as well as theoretical guidance for various practical applications including laser communications, laser warning systems, and remote sensing.

Keywords: atmospheric turbulence, Airy beam, self-repairing, non-diffraction, numerical simulation.

1. Introduction

Light-field amplitude distribution of Airy beams conforms to the Airy function and also satisfies Schrödinger's parabolic equation. Ideal Airy beams exhibit infinite energy, and do not exist in theory. Airy beams show non-diffraction and self-repairing characteristics within a certain propagation distance. The self-repairing effect refers to the fact that beams partially obscured can be recovered to their original pattern after being transmitted over certain distances. These two characteristics of Airy beams are similar to those of Bessel–Gauss (BG) beams. Therefore, it is necessary to make a comparative study of these two characteristics for the Airy and BG beams.

In recent years, numerous scholars have investigated the generation of Airy beams, their propagation characteristics, and applications. Morris *et al*. [1] produced Airy beams with low-coherence, broadband and discussed the dependence relationship of their propagation characteristics on the coherence and wavelengths. Yalong Gu and Gbur [2] investigated the scintillation of an Airy array beam in the atmosphere, which indicated that the array can greatly decrease scintillation with a value close to the the-

oretical minimum obtained. XIUXIANG CHU [3] studied the evolution of Airy beams through atmospheric turbulence, and found that the centroid and self-bending of Airy beams were not influenced by atmospheric turbulence. RUI-PIN CHEN *et al*. [4] proposed the non-diffraction, auto-acceleration, and self-repairing characteristics of Airy beams propagating through free space.

DONGMEI DENG *et al*. [5] studied the energy flows and angular momentum density of non-paraxial Airy beams propagation in free space. XIAOLING JI *et al*. [6] investigated the propagation of Airy beams in the atmosphere (but without turbulence) and considered the influence of thermal blooming on their propagation characteristics. In addition, RUMAO TAO *et al*. [7] investigated the far-field average diffusion of Airy beams through non-Kolmogorov atmospheric turbulence. ROGEL-SALAZAR *et al*. [8] explored the propagation characteristics of Airy beams (without considering the random media). CHUNYI CHEN *et al*. [9] revealed that both mode-locked and mode-unlocked radial Airy array beams exhibit strong self-focusing characteristics after the propagation through atmospheric turbulence. Moreover, WEI WEN *et al*. [10] revealed the propagation characteristics of Airy beams by using Gaussian beams propagating through atmospheric turbulence. Based on the ABCD matrix, the propagation property of an Airy beam from right-handed material (RHM) to left-handed material (LHM) is investigated by LIN HUI-CHUAN and PU JI-XIONG [11].

Scholars have investigated the propagation of Airy beams with the focus on their non-linear (auto-accelerating and self-bending) characteristics in vacuum. At present, most research on the propagation of Airy beams through atmospheric turbulence is aimed at horizontal path propagation. In the laser applications of earth–space–earth and space–earth–space links, including laser communication, laser warning systems, remote sensing, laser radars and laser guidance, laser propagation through atmospheric turbulence along a slant path (turbulence intensity varies with propagation height) are involved. The expression of the light field of beams at $z = L$ (propagation distance) can be calculated by using the ABCD matrix method or Fresnel diffraction integration when beams propagate in free space. However, when beams propagate through atmospheric turbulence, the light field at $z = L$ cannot be expressed because of random fluctuations of the atmospheric refractive index. Therefore, the light-field propagation characteristics of beams can be analyzed by numerical simulation in the absence of experimental conditions. In this work, the split-step Fourier method (SSFM) was applied to simulate Airy and BG beams propagation through atmospheric turbulence along a slant path. Moreover, the self-repairing and non-diffraction characteristics of Airy beams were studied and compared with those of BG beams.

2. Theoretical formulations

The light field of Airy beams at $z = 0$ can be expressed as follows [12, 13]:

$$U(x, y, 0) = \mathrm{Ai}\left(\frac{x}{w_0}\right)\mathrm{Ai}\left(\frac{y}{w_0}\right)\exp\left[\frac{a(x+y)}{w_0}\right] \tag{1}$$

where x, y denote transverse coordinates on the source plane, w_0 and a denote the initial waist radius and truncation parameter, respectively.

The light field of BG beams at $z = 0$ can be expressed as:

$$U_{\mathrm{B}}(r, \varphi, 0) = J_n(\beta r)\exp(-in\varphi)\exp\left(-\frac{r^2}{w_0^2}\right) \tag{2}$$

where $J_n(\beta r)$ represents n-order Bessel function, $\exp(-in\varphi)$ denotes the vortex phase factor, in which n is also the topological charge, $\mathbf{r} = (x, y)$ is the transverse coordinate on the source plane, β is a constant.

The parameter for characterizing turbulence intensity is the refractive index structure constant (RISC) C_n^2 when beams propagate in atmospheric turbulence along a slant path. The Hufnagel–Valley RISC model is used as follows:

$$C_n^2(h) = 0.00594(v/27)^2(10^{-5}h)^{10}\exp(-h/1000) + 2.7\times 10^{-16}\exp(-h/1500) + C_0\exp(-h/100) \tag{3}$$

where h and v represent the propagation height and the wind speed ($v = 21$ m/s), respectively, and $C_0 = 1.7 \times 10^{-14}\ \mathrm{m}^{-2/3}$ refers to the turbulence intensity of the bottom layer. The Kolmogorov spectrum is used, which is expressed as follows:

$$\Phi_n(\kappa) = 0.033 C_n^2 \kappa^{-11/3} \tag{4}$$

where κ refers to the spatial wave number.

3. Split-step Fourier method

It can be seen from the extended Huygens–Fresnel principle [14] that, for a paraxial system in atmospheric turbulence, the field on the receiving plane can be expressed through the source field [15–18]

$$U(\boldsymbol{\rho}, L) = \frac{k}{i2\pi L}\iint_{-\infty}^{\infty} \mathrm{d}^2\mathbf{s}\, U(\mathbf{s}, 0)\exp\left[\frac{ik|\boldsymbol{\rho}-\mathbf{s}|^2}{2L} + \psi(\mathbf{s}, \boldsymbol{\rho})\right] \tag{5}$$

where $\exp[ik|\boldsymbol{\rho} - \mathbf{s}|^2/(2L)]$ represents the phase factor (ignoring fixed phase factor $\exp(ikL)$) such that a spherical wave originates from point $(\mathbf{s}, 0)$ and propagates a distance L to point $(\boldsymbol{\rho}, L)$. Moreover, $\psi(\mathbf{s}, \boldsymbol{\rho})$ refers to the re-phase perturbation of spherical waves in turbulence.

If the intensity fluctuation caused by the turbulence between the source and the receiver is small, it can be neglected, namely, $\psi(\mathbf{s}, \boldsymbol{\rho}) = iS(\mathbf{s}, \boldsymbol{\rho})$. Moreover, $S(\mathbf{s}, \boldsymbol{\rho})$ refers to the light-field phase fluctuation caused by turbulence. When the turbulence is weak enough, the phase fluctuation of the light field can be approximately equivalent to the

phase screen $S(\mathbf{s})$. Thus, Eq. (5) becomes a light wave induced by the previous wave and the fluctuation can be equivalent to a thin screen

$$U(\boldsymbol{\rho}, L) = \frac{k}{i2\pi L}\iint_{-\infty}^{\infty} \mathrm{d}^2\mathbf{s}\, U(\mathbf{s}, 0)\exp\left[\frac{ik|\boldsymbol{\rho}-\mathbf{s}|^2}{2L} + iS(\mathbf{s})\right] \tag{6}$$

After the source field $U(\mathbf{s}, 0)$ passes through the phase screen, the new field formed is $U_s(\mathbf{s}) = U(\mathbf{s}, 0)\exp[iS(\mathbf{s})]$. According to the angular spectrum theory, it can be expanded as the superposition of a series of plane waves

$$U_s(\mathbf{s}) = \frac{1}{(2\pi)^2}\iint_{-\infty}^{\infty} \mathrm{d}^2\boldsymbol{\kappa}\, F(\boldsymbol{\kappa})\exp(i\boldsymbol{\kappa}\cdot\mathbf{s}) \tag{7}$$

where $\boldsymbol{\kappa} = (\kappa_x, \kappa_y, \kappa_z)$, and

$$F(\boldsymbol{\kappa}) = \iint_{-\infty}^{\infty} \mathrm{d}^2\mathbf{s}\, U_s(\mathbf{s})\exp(-i\boldsymbol{\kappa}\cdot\mathbf{s}) \tag{8}$$

Let $E_0(\mathbf{s}, \boldsymbol{\kappa}) = F(\boldsymbol{\kappa})\exp(i\boldsymbol{\kappa}\cdot\mathbf{s})$, then $E_0(\mathbf{s}, \boldsymbol{\kappa})$ can be used to describe the plane wave with an amplitude of $F(\boldsymbol{\kappa})$ and wave vector $\boldsymbol{\kappa} = (\kappa_x, \kappa_y, \kappa_z)$. The following formula can be obtained by substituting Eq. (7) into Eq. (6):

$$U(\boldsymbol{\rho}, L) = \frac{k}{i2\pi L}\iint_{-\infty}^{\infty} \mathrm{d}^2\boldsymbol{\kappa} \iint_{-\infty}^{\infty} \mathrm{d}^2\mathbf{s}\, E_0(\mathbf{s}, \boldsymbol{\kappa})\exp\left(\frac{ik|\boldsymbol{\rho}-\mathbf{s}|^2}{2L}\right) \tag{9}$$

Let

$$E(\boldsymbol{\rho}, \boldsymbol{\kappa}) = \iint_{-\infty}^{\infty} \mathrm{d}^2\mathbf{s}\, E_0(\mathbf{s}, \boldsymbol{\kappa})\exp\left(\frac{ik|\boldsymbol{\rho}-\mathbf{s}|^2}{2L}\right) \tag{10}$$

where $E(\boldsymbol{\rho}, \boldsymbol{\kappa})$ refers to the field of plane wave $E_0(\mathbf{s}, \boldsymbol{\kappa})$ on the receiving plane and Eq. (10) can be written as follows:

$$E(\boldsymbol{\rho}, \boldsymbol{\kappa}_0) = F(\boldsymbol{\kappa}_0)\exp(i\kappa_z L)\exp(i\boldsymbol{\kappa}_0\cdot\boldsymbol{\rho}) \tag{11}$$

where $\kappa_z = \sqrt{\kappa^2 - \kappa_x^2 - \kappa_y^2}$. The field on the receiving plane can be written as

$$U(\boldsymbol{\rho}, L) = \frac{k}{i2\pi L}\iint_{-\infty}^{\infty} \mathrm{d}^2\boldsymbol{\kappa}\, F(\boldsymbol{\kappa})\exp(i\kappa_z L)\exp(i\boldsymbol{\kappa}\cdot\boldsymbol{\rho}) \tag{12}$$

The whole process can be displayed as

$$U(\boldsymbol{\rho}, L) = \mathcal{F}_2^{-1}\left\{\exp(i\kappa_z L)\,\mathcal{F}_2\left[U(\boldsymbol{\rho}_0)\exp(iS(\boldsymbol{\rho}_0))\right]\right\} \tag{13}$$

where $\mathcal{F}_2(\cdot)$ and $\mathcal{F}_2^{-1}(\cdot)$ represent the two-dimensional Fourier transform (FT) and inverse FT, respectively.

When the propagation path is long, the turbulence fluctuates greatly between the emitter and receiver and a large error will be produced in the single phase screen approximation. In this context, the whole path can be divided into multiple intervals, each of which satisfies the single screen approximation, as shown in Eq. (13):

$$U(\boldsymbol{\rho}, z_{j+1}) = \mathcal{F}_2^{-1}\left\{\exp(i\Delta z\kappa_z)\mathcal{F}_2\left[U(\boldsymbol{\rho}', z_j)\exp(iS_j(\boldsymbol{\rho}'))\right]\right\} \tag{14}$$

Thus, the field of the $(j+1)$-th screen can be obtained from that of the j-th screen. In this way, the field on the receiving plane can be acquired from the source field by repeated use of Eq. (14).

Figure 1 shows the SSFM as an iterative process. The two-dimensional FT is involved in Eq. (14), so it is proper to solve the algorithm by using a numerical FT algorithm. The two-dimensional FT and inverse FT can both be calculated by the fast Fourier transform (FFT) during subsequent iterations. Generation of the random phase screen by the spectrum inversion method is an important step [19]. Square phase screen is used in this paper, and the mesh widths in x and y directions are the same. The main parameters involved in the simulation of laser propagation include the mesh width Δx, and Δy that conforms to $\Delta x < \pi/\kappa_{\max}$ ($\kappa_{\max} = [0.045r_0^{-5/3} + 0.025r_0^{-5/3}(k/\Delta z)^{1/6}]^{1/2}$, and r_0 is the coherence length of the atmospheric turbulence, which is a constant when the beam propagates in the atmospheric turbulence along the horizontal path), phase screen width D that satisfies $D > \lambda\Delta z/\Delta x$ [20], and phase screen spacing Δz [18], which are restricted by the variables of turbulence intensity, wavelength, beam width, and have a certain range of values. Due to the beam propagation along a slant path, the

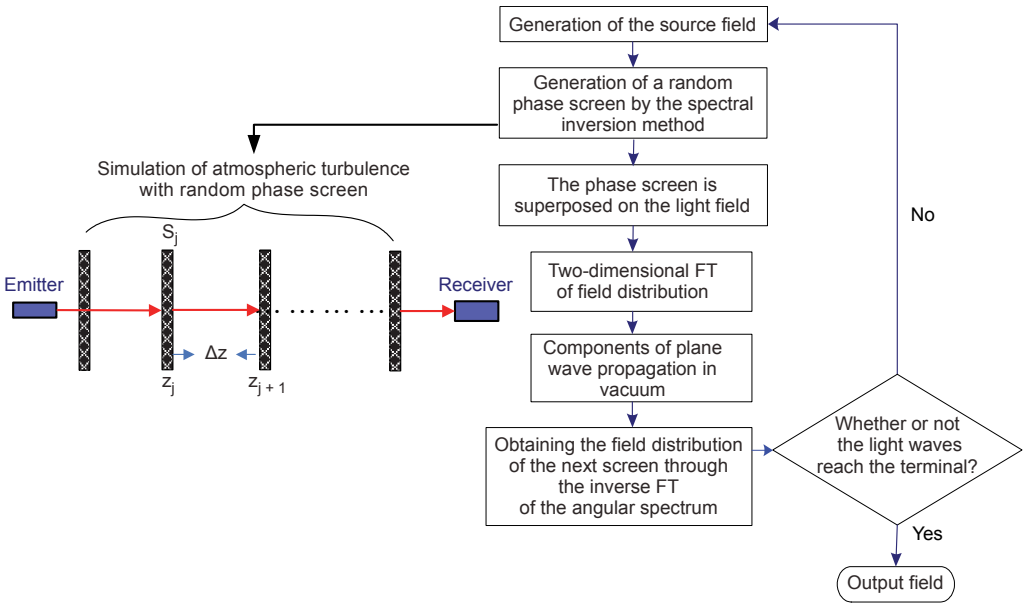

Fig. 1. Flow-process diagram of the split-step Fourier method.

turbulence intensity decreases with the increase of the height, the phase screen spacing is non-uniform.

4. Numerical simulation results

4.1. Self-repairing characteristics of Airy beam propagation

The SSFM was used to simulate Airy beam ($a = 0.1$, $w_0 = 3$ cm) propagation through atmospheric turbulence along a slant path. The parameters used in the simulation were shown in the Table.

In Figure 2, L represents the propagation distance, h refers to the propagation height, and θ is the zenith angle.

The self-repairing characteristic of Airy beams partially obscured was investigated. Supposing that Airy beams are obscured by a Gaussian aperture with size R, then the transfer function can be expressed as $1 - T(x_0, y_0)$, where

$$T(x_0, y_0) = \exp\left(-\frac{x_0^2 + y_0^2}{R^2}\right) \tag{15}$$

Figure 3 shows that the main lobe gradually recovers while side lobes gradually attenuate with increasing propagation distance. In this context, energy is gradually transferred from the side lobes to the main lobe, which conforms to the law of energy conservation. While propagating to a distance of 10 km, the beams can recover their original pattern, namely, they are repaired. During the process of beam repairing, scattered light

T a b l e. Parameter values in the simulation of Airy beam propagation through atmospheric turbulence.

Laser wavelength λ	Structure constant C_0	Phase screen width D	Mesh width Δx	Mesh numbers N	First phase screen spacing Δz
1.06 μm	1.7×10^{-14} m$^{-2/3}$	0.6 m	1.2 m	512	50 m

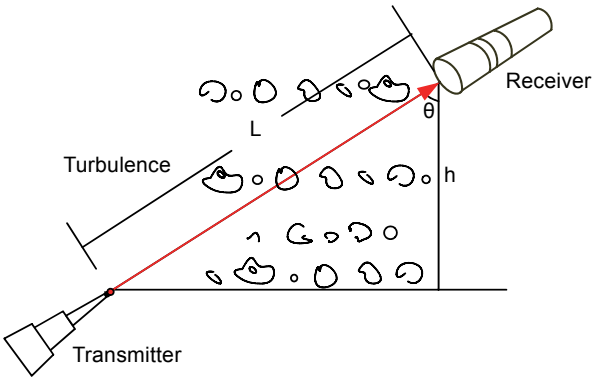

Fig. 2. Diagram of the laser beam propagation through atmospheric turbulence along a slant path.

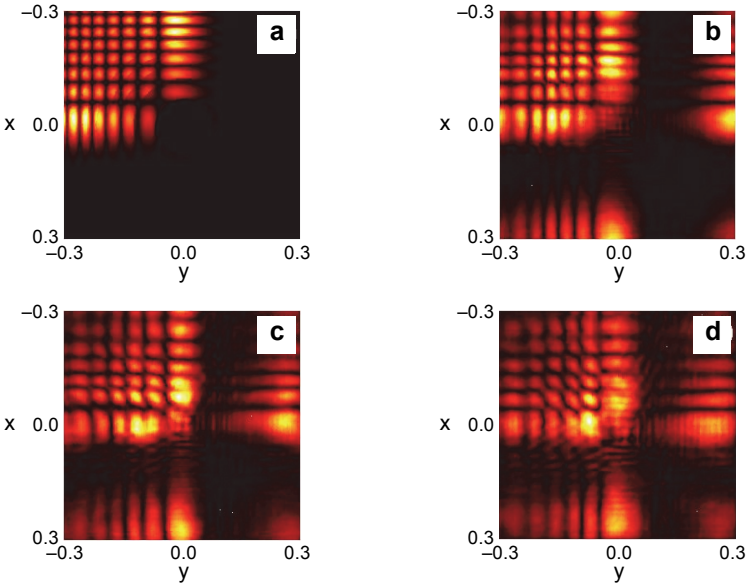

Fig. 3. Self-repairing processes of Airy beams with the main lobe being obscured by a Gaussian aperture propagating in atmospheric turbulence along the horizontal path ($r_0 = 1$); $L = 0$ m (**a**), $L = 5000$ m (**b**), $L = 8000$ m (**c**), and $L = 10000$ m (**d**).

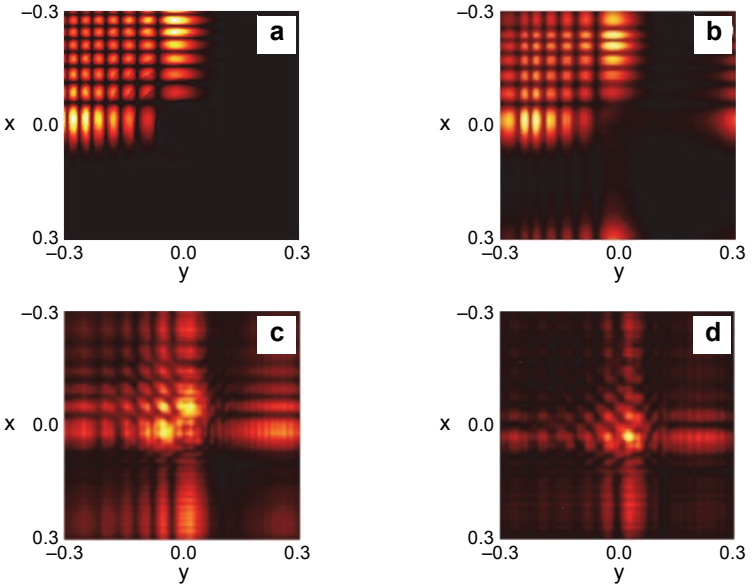

Fig. 4. Self-repairing processes of Airy beams with the main lobe being obscured by a Gaussian aperture propagating in slant atmospheric turbulence ($\theta = 60°$); $L = 0$ m (**a**), $L = 1000$ m (**b**), $L = 2400$ m (**c**), and $L = 2700$ m (**d**).

caused by scattering from the aperture edge is found on the boundary. The beam could not be repaired with the side lobes of the beam being obscured.

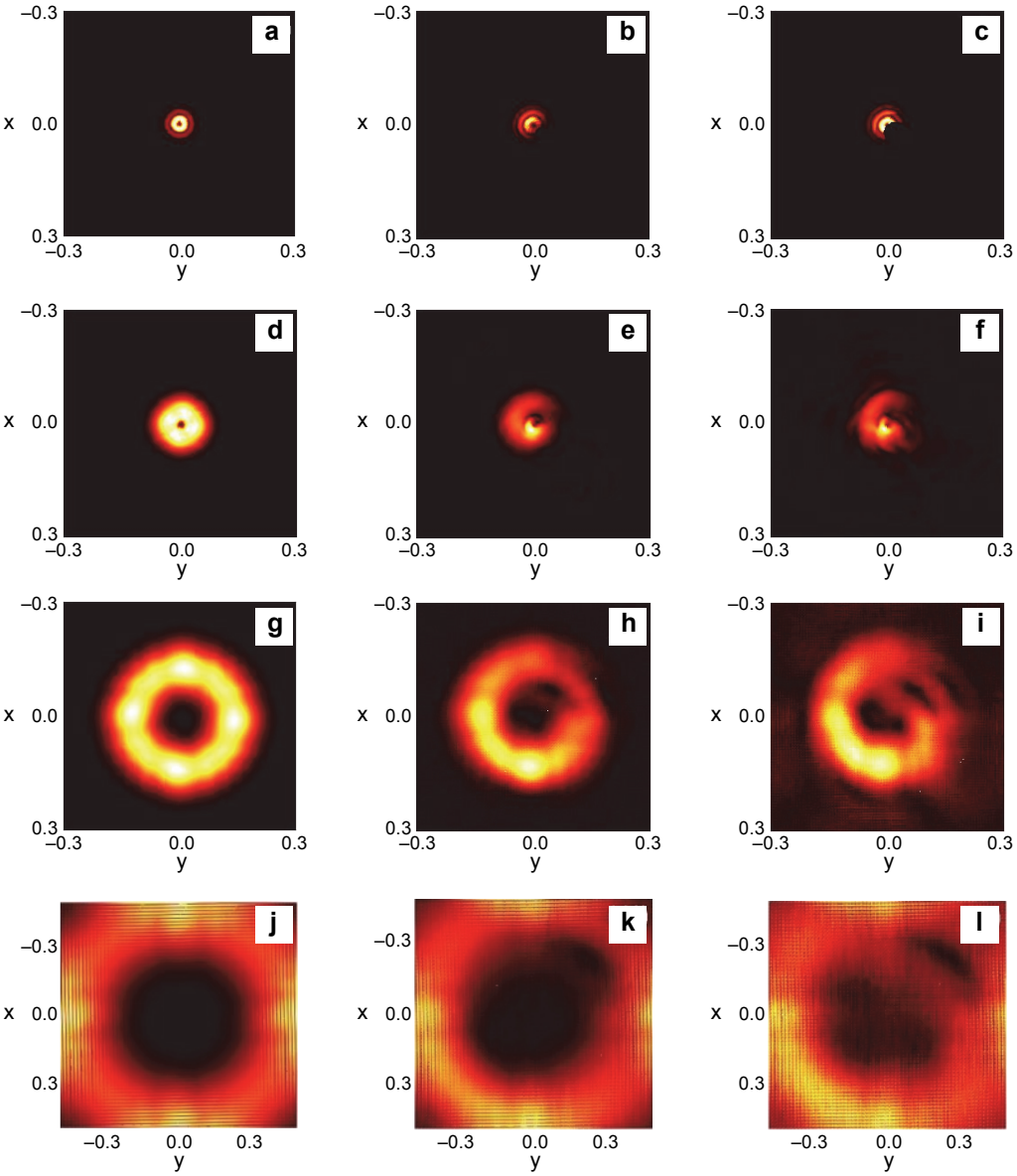

Fig. 5. The field distributions of BG beams without being obscured ($n = 2$, $\theta = 60°$) (**a**, **d**, **g**, **j**); self-repairing processes of BG beams partially obscured by a Gaussian aperture ($R = 1$ cm) (**b**, **e**, **h**, **k**); self-repairing processes of BG beams partially obscured by a Gaussian aperture ($R = 3$ cm) (**c**, **f**, **i**, **l**); $L = 0$ (**a**–**c**), $L = 700$ m (**d**–**f**), $L = 1400$ m (**g**–**i**), and $L = 2700$ m (**j**–**l**).

The beam with the main lobe being obscured by a Gaussian aperture propagation along a slant path in Fig. 4 shows that the process of the energy transformed from the side lobe to the main lobe is the same as the beam propagation in the horizontal path in Fig. 3. The difference is that the beam propagates a shorter distance along a slant path, and reaches the repair state. This is because, turbulence intensity gradually declines with the height at a fixed zenith angle. The influence of turbulence on the beams decreases with increasing propagation distance. When the beam propagates horizontally, the turbulence does not decrease, which indicates that the influence of turbulence on beams increases with increasing propagation distance. Therefore, the influence of atmospheric turbulence on beams propagation along a horizontal path is greater than on beams propagation along a slant path. In other words, the self-repairing characteristic is affected by the zenith angle and turbulence intensity. The beam propagates about 2700 m along a slant path, and it can be repaired. Through numerical simulation, the beams reach their repairing state after propagating for 2400 m with a zenith angle of 30°. The self-repairing characteristic is not affected by the radii of the beam. However, it is affected by the zenith angle and turbulence intensity.

Self-repairing processes of BG beams ($\beta = 200$ m^{-1}, $w_0 = 3$ cm) partially obscured by a Gaussian aperture propagating in slant atmospheric turbulence are studied in Fig. 5.

As shown in Fig. 5, BG beams partially obscured by a Gaussian aperture recover to their previous state after propagating along a slant path for 2700 m. Although the sizes of beams obscured by the Gaussian aperture are different, the repair of the beams is not affected. Also, there is no variation in intensity profile of the beams, *i.e*. the self -repairing and non-diffraction characteristics of the Airy beams are not affected by the radii of the Gauss aperture. In the case of the parameters taken in this work, both of the self-repairing processes of the Airy and BG beams are completed at a propagation distance of about 2700 m.

4.2. Non-diffraction characteristics of Airy beam propagation

The maximum amplitudes of the source light fields of BG and Airy beams without being obscured are normalized. Namely, the initial amplitude of BG beams is equal to that of Airy beams at $L = 0$. A comparison is made between the non-diffraction and self-repairing characteristics of BG and Airy beams when the zenith angle is $\theta = 60°$.

The non-diffraction characteristic refers to that the diffraction spread does not arise in the beam, and the beam profile is invariable within a certain propagation distance. By comparing Figs. 6**a** and 6**b**, it can be seen that Airy beams exhibit an amplitude attenuation while propagating from $L = 0$ to $L = 2700$ m when the beams are not obscured. Moreover, the light-field profile does not change significantly with increasing propagation distance. As shown in Figs. 6**c**–6**f**, after the main lobe of an Airy beam is obscured by a Gaussian aperture, the side lobes have more energy than the main lobe. And the energy is transferred from the side lobes to the main lobe with increasing propagation

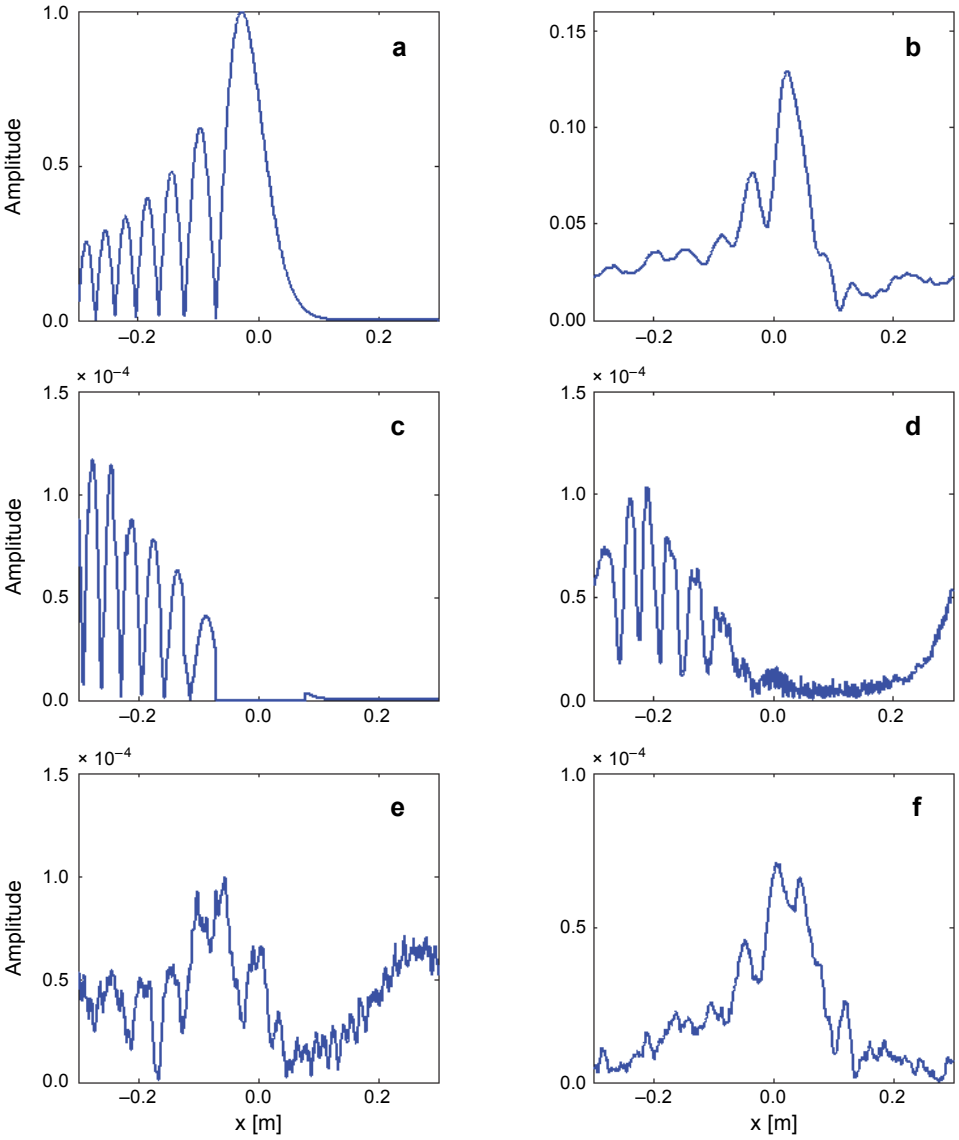

Fig. 6. Variation of maximum amplitude of Airy beams with transverse distance. Normalization of field amplitude of Airy beams without being obscured at $L = 0$ m (**a**), and field-amplitude distribution of Airy beams without being obscured at $L = 2700$ m (**b**). Amplitude distributions of Airy beams with the main lobe being obscured by a Gaussian aperture; $L = 0$ m (**c**), $L = 1000$ m (**d**), $L = 1800$ m (**e**), and $L = 2700$ m (**f**).

distance. Thus, as shown in Fig. 6**f**, at a propagation distance of 2700 m, the amplitude of the main lobe is restored to maximum, while the amplitude profile is basically the same as that in Fig. 6**b**. It indicates that the beams have self-repaired. However, the beam amplitude in Figs. 6**c**–6**f** is four orders of magnitude lower than that in Fig. 6**a**, because the beams are obscured and their energy is reduced.

After comparing Figs. 6 and 7, both Airy and BG beams are repaired at a propagation distance of 2700 m while they have significant difference in non-diffraction and self-repairing characteristics. Moreover, compared Figs. 6**b** with 7**b**, the amplitude attenuation of BG beams without being obscured is greater than that of Airy beams at

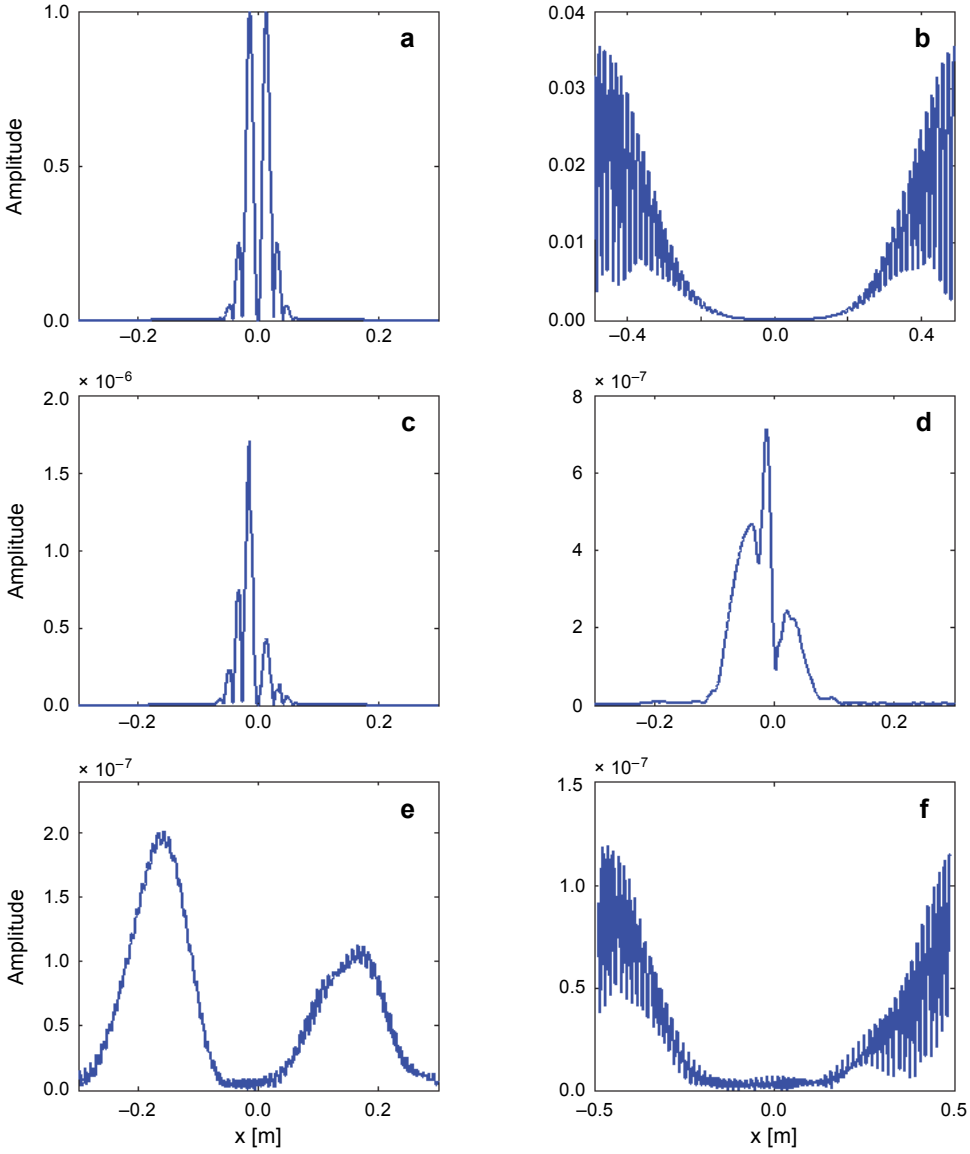

Fig. 7. Variation of maximum amplitude of BG beams with transverse distance. Normalization of field amplitude of BG beams without being obscured at $L = 0$ (**a**), and field-amplitude distribution of BG beams without being obscured at $L = 2700$ m (**b**). Amplitude distributions of the light fields of BG beams with the main lobe being partially obscured by a Gaussian aperture; $L = 0$ m (**c**), $L = 700$ m (**d**), $L = 1400$ m (**e**), and $L = 2700$ m (**f**).

a propagation distance of 2700 m. Figures 7**a** and 7**b** show that the light-field profile of BG beams changes greatly with propagation distance and their non-diffraction characteristics are weaker than those of Airy beams; namely, there is a poor non-diffraction characteristic. As shown in Figs. 7**c**–7**f**, after the BG beam is partially obscured by a Gaussian aperture, the amplitude profile at a propagation distance of 2700 m (Fig. 6**f**) is basically the same as that in Fig. 7**b**. It implies that at 2700 m, BG beams are repaired and the self-repair of which is also a process of energy transfer. However, the amplitude of the beams in Figs. 7**c**–7**f** is six orders of magnitude lower than that in Fig. 7**a** while being two orders of magnitude lower than that in Fig. 6**f**. It can be seen from Figs. 6**f** and 9**d** that the two beams had the same amplitude on the source plane (after normalization) and both were repaired at the same propagation distance. In spite of this, the amplitude of the BG beams was two orders of magnitude lower than that of Airy beams on the receiving plane; namely, the amplitude attenuation of BG beams was larger than that of Airy beams in the process of achieving self-repair. Thus it is noticeable that the quality and stability of the Airy beam propagation in atmospheric turbulence is better than that of the BG beam. The non-diffraction characteristic is affected by the radii of the beams. And the greater the radius, the weaker the non-diffraction effect.

5. Conclusions

Laser beams propagate along a slant path and turbulence intensity gradually decreases with increasing height, so it is necessary to choose non-uniform intervals for phase screens during simulation. The SSFM was used to simulate Airy beam propagation in slant atmospheric turbulence. The results obtained may be summarized as follows.

When an Airy beam (the main lobe being obscured) propagates horizontally for 10 km, the beam is recovered. However, the propagation distance is related to the zenith angle when the self-repairing of an Airy beam propagation along a slant path is achieved. The self-repair of an Airy beam is actually a process of energy transfer from the side lobes to the main lobe.

Airy and BG beams both exhibit non-diffraction and self-repairing characteristics and the two beams (amplitude normalized) obscured by a Gaussian aperture can both be repaired when propagating along a slant path. However, the non-diffraction characteristic of Airy beams is stronger than that of BG beams and the amplitude attenuation of the latter is more serious than that of the former. Therefore, it is better to use an Airy beam than a BG beam in the process of laser transmission.

Results obtained can provide a theoretical basis for outdoor experiment as well as theoretical guidance for various practical applications including laser communications, laser warning systems, and remote sensing.

Acknowledgements – This work was supported by the Scientific Research Program for Key Laboratory Funded by Shaanxi Provincial Education Department (Grant No. 16JS040) and National Natural Science Foundation of China (Grant Nos. 61805190, 11504286, 61271110).

References

[1] Morris J.E., Mazilu M., Baumgartl J., Čižmár T., Dholakia K., *Propagation characteristics of Airy beams: dependence upon spatial coherence and wavelength*, Optics Express 17(15), 2009, pp. 13236–13245.

[2] Yalong Gu, Gbur G., *Scintillation of Airy beam arrays in atmospheric turbulence*, Optics Letters 35(20), 2010, pp. 3456–3458.

[3] Xiuxiang Chu, *Evolution of an Airy beam in turbulence*, Optics Letters 36(14), 2011, pp. 2701–2703.

[4] Rui-Pin Chen, Hong-Ping Zheng, Chao-Qing Dai, *Wigner distribution function of an Airy beam*, Journal of the Optical Society of America A 28(6), 2011, pp. 1307–1311.

[5] Dongmei Deng, Shunli Du, Qi Guo, *Energy flow and angular momentum density of nonparaxial Airy beams*, Optics Communications 289, 2013, pp. 6–9.

[6] Xiaoling Ji, Eyyuboğlu H.T., Guangming Ji, Xinhong Jia, *Propagation of an Airy beam through the atmosphere*, Optics Express 21(2), 2013, pp. 2154–2164.

[7] Ru-mao Tao, Lei Si, Yan-xing Ma, Pu Zhou, Ze-jin Liu, *Average spreading of finite energy Airy beams in non-Kolmogorov turbulence*, Optics and Lasers in Engineering 51(4), 2013, pp. 488–492.

[8] Rogel-Salazar J., Jiménez-Romero H.A., Chávez-Cerda S., *Full characterization of Airy beams under physical principles*, Physical Review A 89(2), 2014, article ID 023807.

[9] Chunyi Chen, Huamin Yang, Kavehrad M., Zhou Zhou, *Propagation of radial Airy array beams through atmospheric turbulence*, Optics and Lasers in Engineering 52, 2014, pp. 106–114.

[10] Wei Wen, Xiuxiang Chu, Haotong Ma, *The propagation of a combining Airy beam in turbulence*, Optics Communications 336, 2015, pp. 326–329.

[11] Lin Hui-Chuan, Pu Ji-Xiong, *Propagation of Airy beams from right-handed material to left-handed material*, Chinese Physics B 21(5), 2012, article ID 054201.

[12] Siviloglou G.A., Christodoulides D.N., *Accelerating finite energy Airy beams*, Optics Letters 32(8), 2007, pp. 979–981.

[13] Siviloglou G.A., Broky J., Dogariu A., Christodoulides D.N., *Observation of accelerating Airy beams*, Physical Review Letters 99(21), 2007, article ID 213901.

[14] Yura H.T., *Mutual coherence function of a finite cross section optical beam propagating in a turbulent medium*, Applied Optics 11(6), 1972, pp. 1399–1406.

[15] Martin J.M., Flatté S.M., *Intensity images and statistics from numerical simulation of wave propagation in 3-D random media*, Applied Optics 27(11), 1988, pp. 2111–2126.

[16] Martin J.M., Flatté S.M., *Simulation of point-source scintillation through three-dimensional random media*, Journal of the Optical Society of America A 7(5), 1990, pp. 838–847.

[17] Flatté S.M., Guang-Yu Wang, Martin J., *Irradiance variance of optical waves through atmospheric turbulence by numerical simulation and comparison with experiment*, Journal of the Optical Society of America A 10(11), 1993, pp. 2363–2370.

[18] Flatté S.M., Gerber J.S., *Irradiance-variance behavior by numerical simulation for plane-wave and spherical-wave optical propagation through strong turbulence*, Journal of the Optical Society of America A 17(6), 2000, pp. 1092–1097.

[19] Flatté S.M., Bracher C., Guang-Yu Wang, *Probability-density functions of irradiance for waves in atmospheric turbulence calculated by numerical simulation*, Journal of the Optical Society of America A 11(7), 1994, pp. 2080–2092.

[20] Nelson D.H., Walters D.L., MacKerrow E.P., Schmitt M.J., Quick C.R., Porch W.M., Petrin R.R., *Wave optics simulation of atmospheric turbulence and reflective speckle effects in CO_2 lidar*, Applied Optics 39(12), 2000, pp. 1857–1871.

Received December 14, 2017
in revised form January 18, 2018